RSC Advances

ROYAL SOCIETY OF CHEMISTRY

www.rsc.org/advances

Journal Name

RSCPublishing

ARTICLE

Preparation and characterization of SiO_2/BiOX (X = Cl, Br, I) films with high visible-light activity

Cite this: DOI: 10.1039/x0xx00000x

Fan Shen[a]†, Li Zhou[a]†, Jiajia Shi[a], Mingyang Xing[a]*, Jinlong Zhang[a]*

Received ooth January 2012,
Accepted ooth January 2012

DOI: 10.1039/x0xx00000x

www.rsc.org/

SiO2/BiOX (X = Cl, Br, I) thin films, which were well adhered to the glass substrates with SiO2 as the intermediate layers, were prepared via a simple sol-gel method. The prepared films were characterized by X-ray diffraction (XRD), Scanning electron microscopy (SEM), UV-visible diffuse reflectance spectroscopy (UV-vis DRS), X-ray photoelectron spectroscopy (XPS) and Raman. The results suggest that the films have tetragonal PbFCl type structure and they crystallized well. These films showed high and stable photocatalytic activity for degradation of RhB under visible light. This method is cheap and convenient, the size and morphology of the product is uniform, production cycle is short, and the process is applicable to large-scale applications. SiO2/BiOX (X = Cl, Br, I) films might have promising application in photocatalysis, photovoltaic film devices, nano-coating, pearlescent pigments and other fields.

1. Introduction

In recent years, the n-type semiconductors have been widely used in the photo-degradation of pollutants, such as TiO_2[1-6], ZnO[7], CdS[8, 9] and so on. Among many semiconductor photocatalysts, TiO_2 is one of the most effective photocatalysts, and many researchers have attempted to study it. However, only UV light can be absorbed by TiO_2 because of its relatively broad band gap (Eg = 3.2 eV), which leads to low utilization of solar energy.[10-12] Therefore, it is necessary to develop a photocatalysts that respond to visible light. Recently, various non-TiO_2-based photocatalysts have been reported by a number of research groups, for example, vanadium (VII) oxide photocatalysts,[13, 14] and bismuth compounds[15-20] and some other visible-light photocatalysts. It is noteworthy that Bi compounds could easily form layered structures due to the special structure of Bi atoms, generating the visible light responsive Bi compounds. In the previous study, Bi is used as a dopant in oxide photocatalysts,[21] but some later studies reported that Bi compounds showed high photocatalytic activity, such as Bi_2O_3[18], Bi_2S_3[19], BiOX (X = Cl, Br, I)[16, 17], BiW_2O_6[15], $BiVO_4$[20] and some of the more complex Bi compounds. Among them BiOX (X = Cl, Br, I) is an excellent visible-light-active photocatalyst with great chemical stability, which worthy of further study.

As a novel and efficient material, BiOX (X = Cl, Br, I) has attracted extensive attention because of its unique internal distribution of electronic structure, optical property and photocatalytic activity. All BiOX (X = Cl, Br, I) compounds have tetragonal PbFCl type crystal structure, and the atomic arrangement consists of tetragonal $[Bi_2O_2]^{2+}$ layers interleaved by double layers of halogen atoms, which interact mainly via Van der Waals forces. Thus, the binding force is so weak that the layered structure could easily dissociate along the [110] directions.[17]

Bismuth oxyhalides have promising application as catalysts, ferroelectric materials and pigments. Bismuth oxyhalides exhibit better performance than TiO_2 (P25) on photocatalytic degradation of organic pollutants. These photocatalysts could respond well to visible light. Hence, bismuth oxyhalides are becoming the hotpots in the field of the photocatalysis. However, bismuth oxyhalides photocatalysts also have a lot of disadvantages, such as the very tiny powder of their nano particles, which leads to the following limitations in large-scale applications. First, the separation of photocatalysts from large volumes of reaction solutions is very difficult.[22] Second, the agglomeration of bismuth oxyhalides could make the particles of catalyst grow up,[23] which might decrease its photocatalytic activity. Third, there is the occurring of catalyst poisoning in suspended phase owing to its poor stability. Fourth, the shadowing effect always exists. Shadowing effect means that the light could be absorbed and scattered by the photocatalysts. Thus the light used in the photocatalytic reaction would be greatly reduced.[24] Making the bismuth oxyhalides to be loaded on a solid substrate to prepare the films with photocatalytic activity could overcome the above mentioned drawbacks. Because the nano-bismuth oxyhalide films could fix the photocatalysts and refine their size, and the photocatalysts would present quantum size effect, small size effect, surface and interface effects, quantum confinement effect and other effects making it possible to further improve their

photocatalytic activity. Therefore, the research shows some theoretical and practical value.

Moreover, SiO_2 films have been widely used in optics, microelectronics and other fields, because some research discovered that they have nice transmittance under visible light and chemical stabilities.[25] In this study, we made SiO_2 as the substrate to combine with the BiOX films. SiO_2 substrate served as isolation layer which could prevent the impurities in the glass from affecting the photocatalytic activity of BiOX films. In addition, BiOX films could grow into different morphologies, which lead to the different photocatalytic activity.

2. Experiment

2.1 Pre-treatment of the glass substrate

A large number of silanol group existing on the surface of the glass could make the glass bond with the coating. However the glass substrate untreated would be polluted due to exposure to air for a long time. Hence, impurities might cover up silanol group, and then prevent the surface from forming films and weaken the adhesive strength between the glass and the coating.[26]

The glass substrates were treated using acid dipping, alcohol washing and ultrasonic cleaning. The method could be briefly described by the following process: 250 mL dilute hydrochloric acid was prepared in a jar, four glass substrates were placed in it and ultrasonic cleaning for 30 min. These glass substrates were taken out and washed by deionized water, and immersed in ethanol and ultrasonic cleaning for 30 min. Then the glass substrates were washed by deionized water, followed by ultrasonic cleaning in deionized water for 30 min. Finally, the cleaned glass substrates were taken out with a tweezers, dried in a constant temperature and humidity oven, sealed and stored. The above lotions must be re-prepared every 2 months. During the process, rubber gloves must be worn, the glass substrates must be put on-down by clean tweezers to avoid polluting the glass substrates.

2.2 Preparation of sols

Preparation of SiO_2 sol. Experimental procedure is shown in Fig. 1, which could be described as the following: 5 g of polyoxyethylene-polyoxypropylene-polyoxyethylene (P123) was dissolved in 25 g of absolute ethanol, and a certain amount of 2 mol/L HCl (0.2 g, 0.4 g, 0.6 g, 0.8 g, 1 g) was added under stirring until complete dissolved at room temperature. Then, 10.4 g of tetraethylorthosilicate (TEOS) was added dropwise to the above solution, which was continuously stirred for 1 h to generate the uniform transparent SiO_2 sol. The prepared sol was aged in an oven with a constant temperature and humidity.

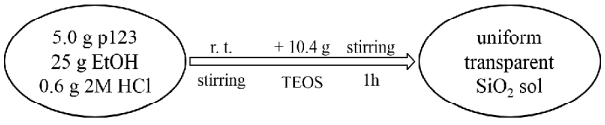

Fig. 1 Preparation of SiO_2 sol.

Preparation of BiOX (X = Cl, Br, I) precursor solution. 11.64 g of Bi_2O_3 (25 mmol) was dissolved in 50 mL of dilute HX (X = Cl, Br, I) solution at room temperature. 0.5-0.4 mL ethylene glycol was added into the above solution under stirring. Then, a small amount of triethanolamine was added and stirred uniformly. BiOX (X = Cl, Br, I) precursor solution was given and stored in an oven with a constant temperature and humidity.

2.3 Preparation of SiO_2/BiOX composite film on the glass substrate

SiO_2/BiOX composite films were located on the glass substrates by using a convenient dip-coating method. The device is simple and the film thickness can be controlled by adjusting the pulling speed, which was limited in 2~5 mm/s. At room temperature (15~30 ^oC), pre-cleaned glass substrates were inserted in SiO_2 sol for 3 min, then it was lifted at the speed of 3 mm/s to form films, followed by calcination at 350 ^oC for 2 h. The obtained films were immersed in BiOX (X = Cl, Br, I) precursor solution for 3 min, then were lifted at the speed of 3 mm/s to form films. Finally, the given films were dried at 50 ^oC in the oven to generate SiO_2/BiOX composite films.

2.4 Characterization

XRD analysis of the prepared films were carried out with a Rigaku D/max 2550 VB/PC apparatus using Cu Kα radiation (λ = 1.54056 Å), Ni as filter, operated at 40 kV and 100 mA, in the range of 10-80°. Scanning electron microscopy (SEM, JEOL USA, JSM-6360, voltage 15KV) was used to observe the morphology of films surface. The prepared films were cut into small pieces with glass cutter, and gold was gilded on every small piece, which was fixed by double-sided adhesive. This characterization was carried out in SEM test chamber. UV-Vis absorption spectra were recorded with a scan UV-Vis spectrophotometer (Varian Cary 500), while $BaSO_4$ was used as a reference, and the measuring range was 400-800 nm. X-ray photoelectron spectroscopy (XPS) was obtained by using a Perkin-Elmer PHI 5000C ESCA System with Mg Kα radiation operated at 300 W.

2.5 Photocatalysis test

The prepared SiO_2/BiOX (X = Cl, Br, I) films (effective size of the films is 25 mm× 33 mm) were vertically added in glass tubes containing 60 mL rhodamine B solution (10 $mg \cdot L^{-1}$, RhB), and the distance between the glass tube and the light source is 25 cm. An iodine tungsten lamp was used as the light source, and the wavelength of the light through the filter was higher than 420 nm. The mixture was stirred for 30 min in the dark until absorption-desorption equilibrium, and then put into the photocatalytic reactor. The surface of films must be perpendicular to the light source, illumination time was 240 min, and the analytical samples were taken from the mixture every 60 min. The concentration of the solution was analyzed by checking the absorbance at 553 nm with a UV-vis spectrophotometer (Shimadzu UV-2450).

3. Results and Discussion

3.1 XRD characterization

XRD characterization could be used to check the composition and structure of the sample. However, it could be difficultly carried out, because the thickness of films was less than 400 nm. The peaks of films might coincide with the peaks of the glass, and the peaks would be very low. In the analysis, precursor solution was used to generate the powder for XRD to observe the crystal phase structures of the prepared films. The XRD patterns of the powder given by BiOX (X = Cl, Br, I) precursor solution (Fig. 2) show that the powder possesses high degree of crystallinity with space groups of P4/nmm and tetragonal PbFCl type structure.[17]

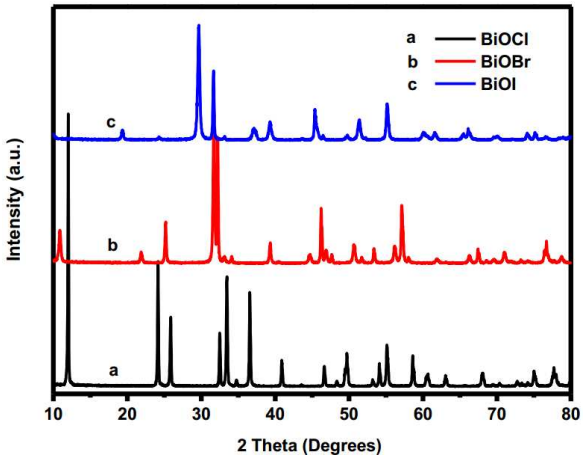

Fig. 2 XRD patterns of BiOX (X = Cl, Br, I) powder: (a) BiOCl; (b) BiOBr; (c) BiOI.

Table 1 The crystalling phase structure of BiOX (X = Cl, Br, I)

photocatalyst	PDF	structure	space group	cell parameter/nm	particle size/nm
BiOCl	06-0249	tetragonal	P4/nmm	a=b=0.3894, c=0.7369	34.1
BiOBr	09-0393	tetragonal	P4/nmm	a=b=0.3924, c=0.8101	27.2
BiOI	10-0445	tetragonal	P4/nmm	a=b=0.3992, c=0.9151	24.5

Sherrer equation could be used to figure out the particle size:[27]

$$D = \frac{K\lambda}{\beta \cos\theta} \qquad (1)$$

where K = 0.89, λ = 1.54056 Å, β = B - 0.1, B is the half width of the highest peak (in rad), D is the estimated particle size (in Å). The particle size of these three samples could be estimated to be 34.1 nm, 27.2 nm, 24.5 nm (listed in Table 1), indicating that from BiOCl, BiOBr to BiOI, the particle size of BiOX (X = Cl, Br, I) gradually decreased. The standard peak of BiOX (X = Cl, Br, I) was respectively compared with its powder sample, and the result was shown in Fig. 3. From XRD patterns of each sample, we can see that every sample has strong diffraction peaks, and no impure peaks exist, which indicates that they exhibit high degree of crystallinity. As shown in Fig. 3a, the diffraction peaks of BiOCl are consistent with BiOCl in Standard Library of Spectra (JCPDS No.06-0249). The crystal plane index of the three highest peaks are (001), (002) and (102), whose unit cell parameter is a = b = 0.3894, c = 0.7369 with tetragonal PbFCl type structure. The absence of the peaks ascribed to the impurity indicates that the BiOCl sample obtained by this method possesses high purity. In the same way, Fig. 3b and Fig. 3c respectively correspond to BiOBr (JCPDS No. 09-0393) and BiOI (JCPDS No.10-0445), they all present high purity and crystallinity. These results show that BiOX (X = Cl, Br, I) could be well prepared by this convenient method. Details of crystal structures and lattice parameters of BiOX (X = Cl, Br, I) are listed in Table 1.

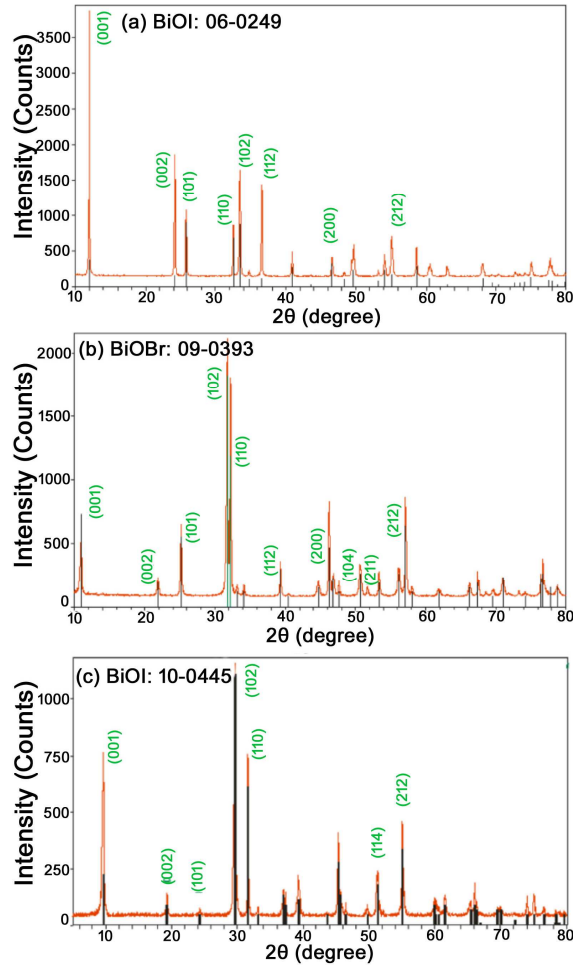

Fig. 3 XRD patterns of BiOX (X = Cl, Br, I) powder contrasts with its standard peak: (a) BiOC: 06-0249l; (b) BiOBr: 09-0393; (c) BiOI: 10-0445.

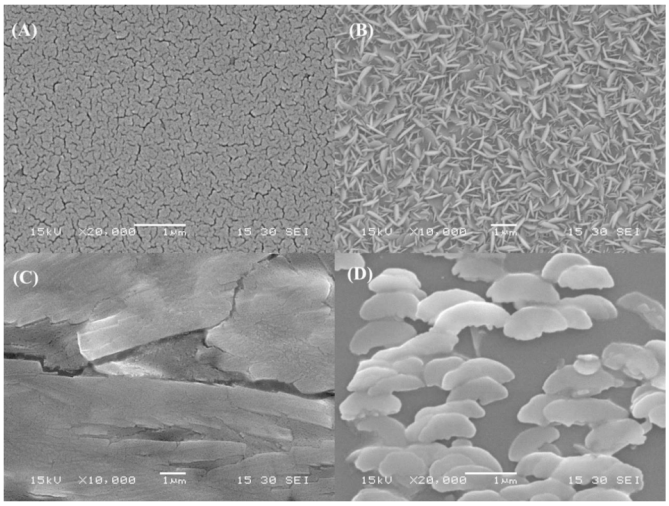

Fig. 4 SEM images of SiO_2/BiOX (X = Cl, Br, I) samples: (A) SiO_2 thin film; (B) SiO_2/BiOCl thin film; (C) SiO_2/BiOBr thin film; (D) SiO_2/BiOI thin film.

3.2 SEM characterization

SiO_2/BiOX (X = Cl, Br, I) thin films are cut into small pieces with glass cutter for SEM characterization, and the results are shown in Fig. 4. Fig. 4A shows the SEM image of a single layer of SiO_2 film, revealing that the layer is dense and drying crack. Fig. 4B is the SEM of SiO_2/BiOCl thin film, indicating that BiOCl layer possesses nice uniformity and dispersibility with lamellar structure, and the thickness is about 50 nm. The sheet-like structure is consistent with related literatures[17]. SiO_2/BiOBr thin film just exhibits the layered plate structure (Fig. 4C), and the fan-like structure can be observed from the SEM of SiO_2/BiOI film (Fig. 4D). In general, SiO_2/BiOX (X = Cl, Br, I) thin films all possess different layered structures, because crystals would grow along the different directions due to the different halogen atoms. The various morphologies are expected to give different photocatalytic activity owing to the difference of light adsorption, transmission and composite of surface electrons.

3.3 XPS characterization of SiO_2/BiOX (X = Cl, Br, I) films

XPS characterization could be used to analyze the valence of each element in the sample, thus the peak separation of XPS spectra of Bi and X (X = Cl, Br, I) is shown in Fig. 5. As shown in Fig. 5a, the peaks with the binding energy of 165.1 eV and 159.8 eV are corresponding to Bi $4f_{5/2}$ and Bi $4f_{7/2}$ in BiOCl. The Cl $2p_{3/2}$ peak is at 198.8 eV (Fig. 5b). The data of the other elements are listed in Table 2, Bi $4f_{5/2}$, Bi $4f_{7/2}$ and halogen atoms are consistent with related literatures,[28-30] indicating that the samples prepared are BiOX (X = Cl, Br, I) crystals, in which all Bi is in the Bi^{+3} state and X in the X^{-1} state.

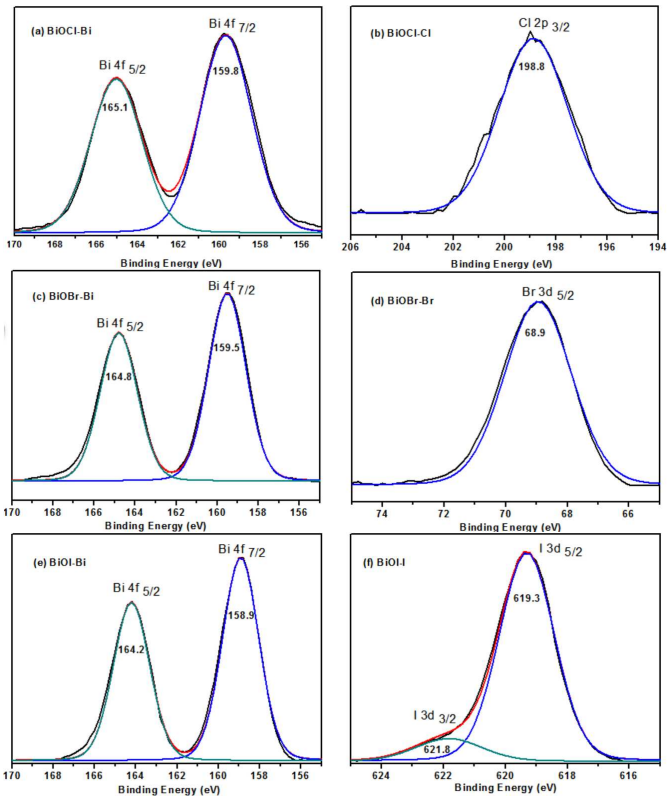

Fig. 5 XPS spectra of the BiOX (X = Cl, Br, I) powder: (a) BiOCl-Bi; (b) BiOCl-Cl; (c) BiOBr-Bi; (d) BiOBr-Br; (e) BiOI-Bi; (f) BiOI-I.

Table 2 XPS data of the BiOX (X = Cl, Br, I) powder

Photocat-alysts	Bi $4f_{5/2}$/eV	Bi $4f_{7/2}$/eV	X/eV	O 1s/eV	O 1s/eV	Ref.
BiOCl	165.1	159.8	Cl $2p_{3/2}$198.8	531.2	533.6	[28]
BiOBr	164.8	159.5	Br $3d_{5/2}$68.9	530.6	532.6	[29]
BiOI	164.2	158.9	I $3d_{5/2}$619.3 I $3d_{3/2}$621.8	530.2	532.7	[30]

Table 3 Band gap data of the BiOX (X = Cl, Br, I) powder

photocatalysts	E_g/eV	E_{cb}[a]/eV	E_{vb}[b]/eV	λ_g/nm
BiOCl	3.2	0.26	3.45	370
BiOBr	2.75	0.48	3.23	440
BiOI	1.76	0.56	2.32	685

[a] E_{cb} stands for the position of the conduction band of BiOX. [b] E_{vb} stands for the position of the valence band of BiOX.

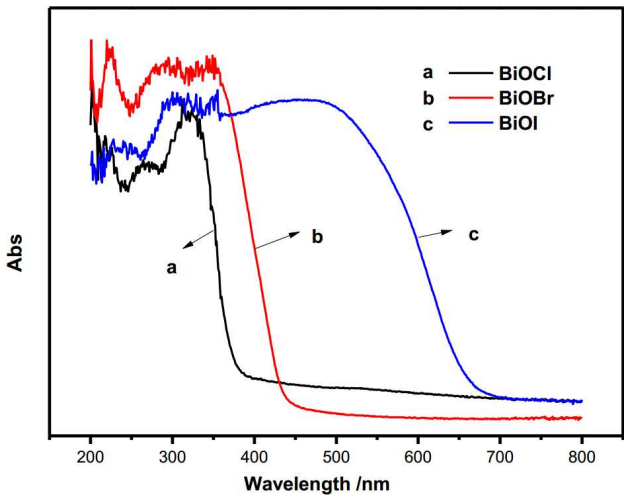

Fig. 6 UV-vis diffuse reflectance spectra of BiOX (X = Cl, Br, I) powder: (a) BiOCl (b) BiOBr (c) BiOI.

3.4 DRS characterization of the SiO_2/BiOX (X = Cl, Br, I) film

UV-Vis DRS was carried out to study the absorption of SiO_2/BiOX (X = Cl, Br, I) thin films, and the result is shown in Fig. 6. UV-Vis DRS is often used to check the optical absorption properties of materials. From Fig. 6, with the increment of halogen atomic number, the light absorption range of the sample increases, and the corresponding band gap decreases. Especially BiOI presents a strong absorption under visible light. Intrinsic absorption coefficient "α" of the semiconductors is the function between the wavelength of incident light and the type of solid band transitions, and the relationship between α and photon energy $h\upsilon$ could be expressed as:[31]

$$\alpha h\upsilon = A(h\upsilon - E_g)^{n/2} \quad (2)$$

where A is a constant, n depends on the type of transition type, n = 1 with direct transition, n = 4 with indirect transition, thus in BiOX, n = 4. The band gap could be estimated with formula (2). The conduction band could be estimated with formula (3).[32] Furthermore, band structure would be analyzed, and the result is listed in Table 3.

$$E_{CB} = X - E_C + 0.5E_g \quad (3)$$

where X is the absolute electronegativity of the semiconductor, E_C is the energy of free electrons on the hydrogen scale. Table 3 shows that the band gap tends to decrease with the increment of the halogen atomic number, revealing that the ability of absorbing visible light gradually improves, which could be visually distinguished. BiOCl is white, BiOBr is yellow, while BiOI is red. Calculations show that valence band getting smaller and smaller from BiOCl, BiOBr to BiOI. Thus, the oxidative ability gradually decreases, which will be discussed in detail in the mechanism of photocatalytic degradation in below.

3.5 Raman spectra of BiOCl

BiOCl was reported to have a tetragonal PbFCl type structure consists of $[Bi_2O_2]^{2+}$ layers and double layers of Cl atoms.[17] From the Raman spectra (Fig. 7), the peak at 141 cm^{-1} can be assigned to the stretching vibration A_{1g} of Bi-Cl, the peak at 197 cm^{-1} is attributed to the stretching vibration of Bi-Cl, and the peak at 396 cm^{-1} is caused by the vibration of Bi-O. The above result can further confirm the sample to be BiOCl.

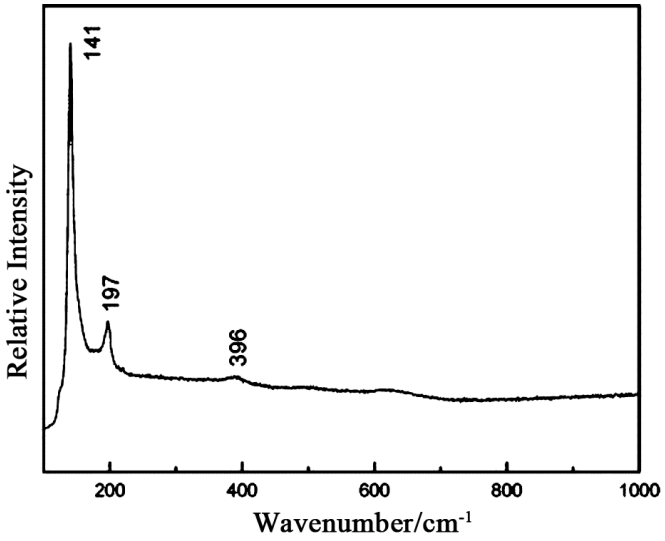

Fig. 7 Raman spectra of BiOCl.

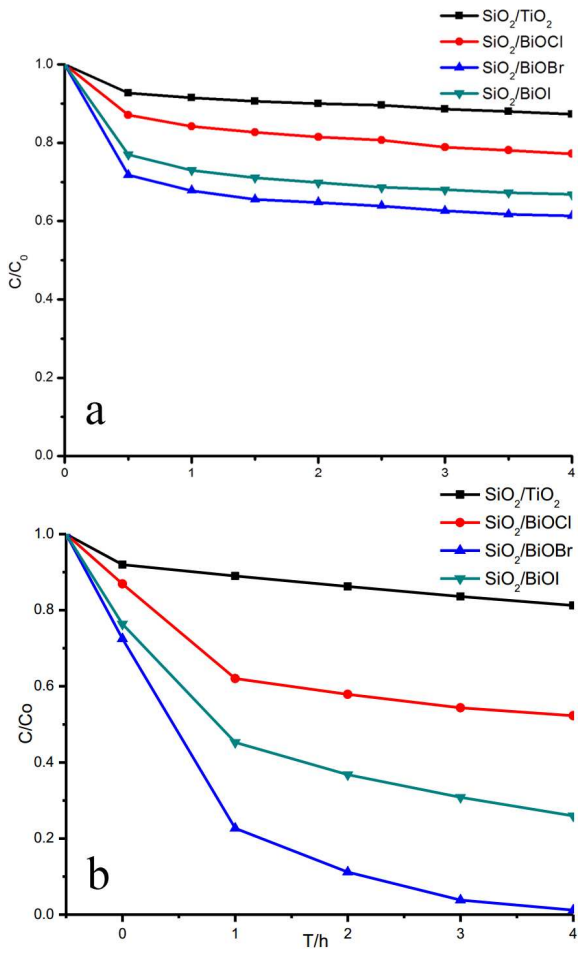

Fig. 8 Adsorbability (a) and photocatalytic activity (b) of the different thin films for RhB.

3.6 Photocatalytic activity of the thin film

Fig. 8(a) shows the adsorbability of the prepared thin filmsfor RhB. After 0.5 h in the dark, the adsorbability showed relatively stable trend. Fig. 8(b) shows that the concentration of RhB decreased more sharply in the illumination condition. SiO_2/BiOBr exhibits the highest photocatalytic activity, and its degradation rate reached 98% at the optimal condition of 3h. BiOX (X = Cl, Br, I) films are all superior to SiO_2/TiO_2 film in photocatalytic activity. The ranking order of the degradation activity to RhB is: SiO_2/BiOBr > SiO_2/BiOI > SiO_2/BiOCl.

The reasons can be analyzed in two ways. On the one hand, the larger the valence band of the semiconductor is, the stronger oxidative ability would be.[33] From Table 3, from BiOCl, BiOBr to BiOI, the valence band gradually decreases, so the ranking of the oxidative ability is: BiOCl > BiOBr > BiOI. On the other hand, photocatalytic reaction necessitates the excitation of the semiconductor by absorbing photons.[34] Thus, the absorption capability of visible light could also affect the photocatalytic activity.[35] From Table 3, with the halogen atomic number increasing, the band gap of BiOX decreases, showing that the visible light absorption capacity gradually increases. Thus the photocatalytic efficiency rises. The ranking of visible light absorption capacity is: BiOI > BiOBr > BiOCl. Comprehensive consideration of these two competing factors, the ranking order of degradation activity to RhB of SiO_2/BiOX (X = Cl, Br, I) under visible light is: SiO_2/BiOBr > SiO_2/BiOI > SiO_2/BiOCl.

3.7 Mechanism of photocatalytic degradation

At the optical condition, three possible mechanisms might explain the degradation of the dye on the surface of the semiconductor. In addition to the semiconductor photocatalytic mechanism, the dye-sensitized mechanism and dye-photolysis mechanism also probably exist.

The dye-sensitized mechanism means that dye is excited by light to form excited states, and the electrons in the excited states are transferred to the conduction band of photocatalyst leading to electron injection.[36] Then the electrons and O_2 in the water could be combined to form $\cdot OOH/\cdot O_2^-$ group, which has high oxidative activity.[37] As a result, the high-activity group could degrade the dye. Dye-photolysis mechanism can be described that the dye is excited by light to form excited states,[38] then the electrons in the excited states could be combined with O_2 in the water to form $\cdot O_2^-$ high-activity group, which could degrade the dye. RhB is chemically stable, and the concentration cannot be detected reducing in the absence of catalysts. Thus in this study the self-degradation mechanism could be ignored.

In general, deethylation is accompanied with ring-opening reaction of benzene rings during the photocatalytic degradation of RhB.[39] During photocatalytic process of films, deethylation plays a dominant role, while ring-opening reaction could be secondary.[40] RhB (λ_{max} = 553 nm) could generate Rhodamine (λ_{max} = 498 nm) via deethylation in the photocatalytic reaction. With the photocatalytic reaction, deethylation are continually carried out. For de-ethyl RhB, benzene rings are constantly attacked by ·OH till the complete degradation of molecules. The blue-shift of the maximum absorption peak could correspond to the deethylation of RhB. With the deethylation by step, the absorption peak was gradually blue-shifted from 553 nm to 552 nm, then to 510 nm, finally to 498 nm, which was observed directly with its colour gradually turned from red to yellow.

The photocatalytic activity of the semiconductors intrinsically depends on electronic structures,[41] because the photocatalytic activity is closely related to the conduction band (CB) and the valence band (VB), as well as the mobility of carriers. CB and VB, respectively, could determine the oxidative ability and reductive ability of the catalyst, while the mobility of carriers could determine the photocatalytic efficiency. For metal oxide photocatalysts, the VB consists of 2p orbit of oxygen, but for bismuth-based semiconductors, the VB is hybridized by 2p orbit of oxygen and 6s orbit of Bi, and the CB is composed of 6p orbit of Bi,[42] which possesses high reductive activity.

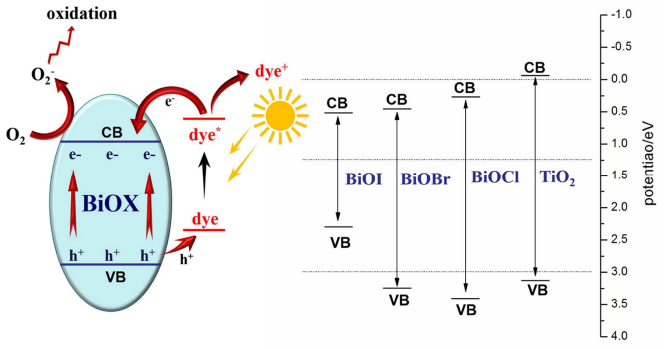

Fig. 9 The level position of BiOX (X = Cl, Br, I) and photocatalytic degradation mechanism of RhB.

Among bismuth oxyhalides, BiOCl is an indirect wide band-gap semiconductor. O_{2p} orbit and Cl_{3p} orbit occupy its VB,[43] and the CB consist of Bi_{6p} orbit. From DRS data, the band gap of BiOCl is 3.2 eV, so it should only have UV activity. However, the result of the photocatalytic degradation indicates that BiOCl also shows activity under visible light. We think that in this experiment, the photocatalytic degradation of RhB on BiOCl was attributed to the dye-sensitized mechanism (Fig. 9). Meanwhile, during the photocatalytic degradation, with the gradual fading of the color of solution, the photosensitization effect decreased, which would slow the photocatalytic degradation (Fig. 8). For BiOBr and BiOI, their band gaps are respectively 2.75 eV and 1.76 eV, so visible light can be absorbed. Thus, the photocatalytic degradation might include both photocatalysis and photosensitization. BiOBr had the highest photocatalytic activity with the appropriate CB and VB, as well as a nice response to the visible light.

According to some literatures, visible light activity of SiO_2/BiOX (X = Cl, Br, I) attributes to their layered structures,

the halogen atoms X exist between the $[Bi_2O_2]$ layers.[17] $[Bi_2O_2]$, [X], $[Bi_2O_2]$ would stack along the c axis to form special layered structures. Bi atoms in this structure possess two states. One exhibits distorted $[BiO_4]$ polyhedrons, and another shows distorted $[BiO_4X_4]$ polyhedrons. These layered structures with partial distorted polyhedrons are beneficial to the electronic transfer and photocatalytic property.

3.8 Repeatability of films

In order to investigate the stability of the photocatalytic films, SiO_2/BiOCl film was continuously used for 4 times (Fig. 10). The photocatalytic activity was only slightly decreased, indicating a firm adhesion between the prepared films and substrates. The stable visible photocatalytic activity could fulfil the continuous usage in the actual water degradation process.

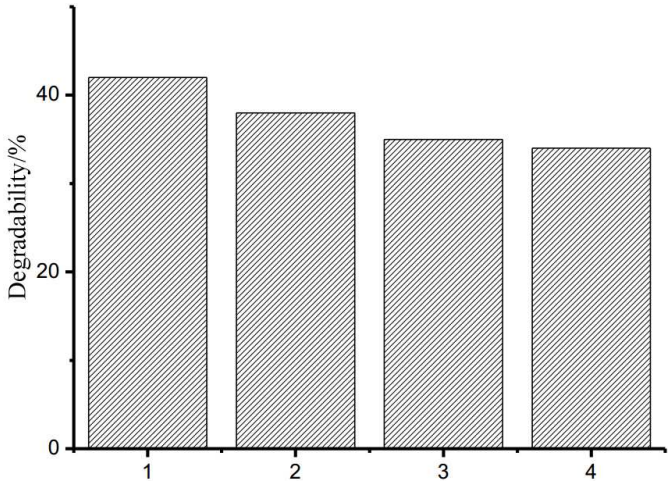

Fig. 10 Repeatability of photocatalytic activity of SiO_2/BiOCl thin films.

Conclusions

SiO_2/BiOX (X = Cl, Br, I) thin films with layered structures were prepared via a convenient sol-gel method. The films have high and stable photocatalytic activity under visible light irradiation. SiO_2/BiOX (X = Cl, Br, I) thin films have tetragonal PbFCl type structure, and the sample crystallized well and stably. In addition, with the increment of the halogen atomic number, the particle size gradually decreases. The results of DRS and photocatalytic activity test indicated that the sample could respond well to visible light. SiO_2/BiOBr thin film showed the highest photocatalytic activity under visible light. Furthermore, SiO_2/BiOX (X = Cl, Br, I) thin films presented higher photocatalytic activity than TiO_2 film. The ranking of degradation activity of SiO_2/BiOX (X = Cl, Br, I) under visible light is: SiO_2/BiOBr > SiO_2/BiOI > SiO_2/BiOCl. Two factors affect their photocatalytic activity: the energy band structure and the light absorption ability.

Acknowledgements

This work has been supported by National Nature Science Foundation of China (21237003, 21173077, 21377038, 21073060, 21203062), the National Basic Research Program of China (973 Program, 2013CB632403), the Research Fund for the Doctoral Program of Higher Education(20120074130001) the Fundamental Research Funds for the Central Universities.

Notes and references

† Fan Shen and Li Zhou have contributed equally to this work.

[a] Key Laboratory for Advanced Materials and Institute of Fine Chemicals, East China University of Science and Technology, 130 Meilong Road, Shanghai 200237, P.R. China

* Email: mingyangxing@ecust.edu.cn; jlzhang@ecust.edu.cn`

1. M. R. Hoffmann, S. T. Martin, W. Choi and D. W. Bahnemann, *Chem. Rev.*, 1995, **95**, 69-96.
2. M. Xing, J. Zhang and F. Chen, *J. Phys. Chem. C*, 2009, **113**, 12848-12853.
3. B. Qiu, M. Xing and J. Zhang, *J. Am. Chem. Soc.*, 2014, **136**, 5852-5855.
4. M. Xing, W. Fang, M. Nasir, Y. Ma, J. Zhang and M. Anpo, *J. Catal.*, 2013, **297**, 236-243.
5. M. Takeuchi, M. Matsuoka and M. Anpo, *Res. Chem. Intermediat.*, 2012, **38**, 1261-1277.
6. N. Negishi and K. Takeuchi, *Res. Chem. Intermediat.*, 2003, **29**, 861-879.
7. S. Chakrabarti and B. K. Dutta, *J. Hazard. Mater.*, 2004, **112**, 269-278.
8. Z. Gao, N. Liu, D. Wu, W. Tao, F. Xu and K. Jiang, *Appl. Surf. Sci.*, 2012, **258**, 2473-2478.
9. Y. Huo, X. Yang, J. Zhu and H. Li, *Appl. Catal. B*, 2011, **106**, 69-75.
10. R. Asahi, T. Morikawa, T. Ohwaki, K. Aoki and Y. Taga, *Science*, 2001, **293**, 269-271.
11. J. Zhang, Y. Wu, M. Xing, S. A. K. Leghari and S. Sajjad, *Energ Environ. Sci.*, 2010, **3**, 715-726.
12. M. Xing, J. Zhang and F. Chen, *Appl. Catal. B*, 2009, **89**, 563-569.
13. R. Shi, Y. Wang, F. Zhou and Y. Zhu, *J. Mater. Chem.*, 2011, **21**, 6313-6320.
14. H. Guo, J. Chen, W. Weng and S. Li, *Appl. Surf. Sci.*, 2011, **257**, 3920-3923.
15. H. Fu, C. Pan, W. Yao and Y. Zhu, *J. Phys. Chem. C*, 2005, **109**, 22432-22439.
16. J. Henle, P. Simon, A. Frenzel, S. Scholz and S. Kaskel, *Chem. Mater.*, 2007, **19**, 366-373.
17. X. Zhang, Z. Ai, F. Jia and L. Zhang, *J. Phys. Chem. C*, 2008, **112**, 747-753.
18. L. Zhou, W. Wang, H. Xu, S. Sun and M. Shang, *Chem. Eur. J.*, 2009, **15**, 1776-1782.
19. Y. Wang, J. Chen, P. Wang, L. Chen, Y.-B. Chen and L.-M. Wu, *J. Phys. Chem. C*, 2009, **113**, 16009-16014.
20. A. Kudo, K. Omori and H. Kato, *J. Am. Chem. Soc.*, 1999, **121**, 11459-11467.
21. K. Lv, H. Zuo, J. Sun, K. Deng, S. Liu, X. Li and D. Wang, *J. Hazard. Mater.*, 2009, **161**, 396-401.
22. L. Zhang, W. Wang, L. Zhou, M. Shang and S. Sun, *Appl. Catal. B*, 2009, **90**, 458-462.
23. F. I. López-Salinas, G. A. Martínez-Castañón, J. R. Martínez-Mendoza and F. Ruiz, *Mater. Lett.*, 2010, **64**, 1555-1558.
24. H. M. Coleman, C. P. Marquis, J. A. Scott, S. S. Chin and R. Amal, *Chem. Eng. J.*, 2005, **113**, 55-63.
25. Y. Kim, F. Zhao, M. Mitsuishi, A. Watanabe and T. Miyashita, *J. Am. Chem. Soc.*, 2008, **130**, 11848-11849.
26. P. C. Hidber, W. Helbig, E. Kim and G. M. Whitesides, *Langmuir*, 1996, **12**, 1375-1380.
27. A. L. Patterson, *Phys. Rev.*, 1939, **56**, 978-982.
28. F. Dong, Y. Sun, M. Fu, Z. Wu and S. C. Lee, *J. Hazard. Mater.*, 2012, **219–220**, 26-34.

29. J. Xia, S. Yin, H. Li, H. Xu, L. Xu and Y. Xu, *Dalton T.*, 2011, **40**, 5249-5258.
30. X. Zhang, L. Zhang, T. Xie and D. Wang, *J. Phys. Chem. C*, 2009, **113**, 7371-7378.
31. A. E. Morales, E. S. Mora and U. Pal, *Rev. Mex. Fis. S*, 2007, **53**, 18.
32. Y. Xu and M. A. Schoonen, *Am. Mineral*, 2000, **85**, 543-556.
33. D. Lawless, N. Serpone and D. Meisel, *J. Phys. Chem.*, 1991, **95**, 5166-5170.
34. H. Shi, J. Chen, G. Li, X. Nie, H. Zhao, P.-K. Wong and T. An, *ACS Appl. Mater. Interfaces*, 2013, **5**, 6959-6967.
35. A. Heller, *Accounts Chem. Res.*, 1995, **28**, 503-508.
36. R. Katoh, A. Furube, A. V. Barzykin, H. Arakawa and M. Tachiya, *Coordin. Chem. Rev.*, 2004, **248**, 1195-1213.
37. H. Shi, G. Li, H. Sun, T. An, H. Zhao and P.-K. Wong, *Appl. Catal. B*, 2014, **158–159**, 301-307.
38. Y. Xie and C. Yuan, *Appl. Catal. B*, 2003, **46**, 251-259.
39. T. Wu, G. Liu, J. Zhao, H. Hidaka and N. Serpone, *J. Phys. Chem. B*, 1998, **102**, 5845-5851.
40. J. Zhuang, W. Dai, Q. Tian, Z. Li, L. Xie, J. Wang, P. Liu, X. Shi and D. Wang, *Langmuir*, 2010, **26**, 9686-9694.
41. M. Sathish, B. Viswanathan, R. P. Viswanath and C. S. Gopinath, *Chem. Mater.*, 2005, **17**, 6349-6353.
42. J. Tang, Z. Zou and J. Ye, *Angew. Chem. Int. Ed.*, 2004, **43**, 4463-4466.
43. C. Wang, C. Shao, Y. Liu and L. Zhang, *Scripta Mater.*, 2008, **59**, 332-335.

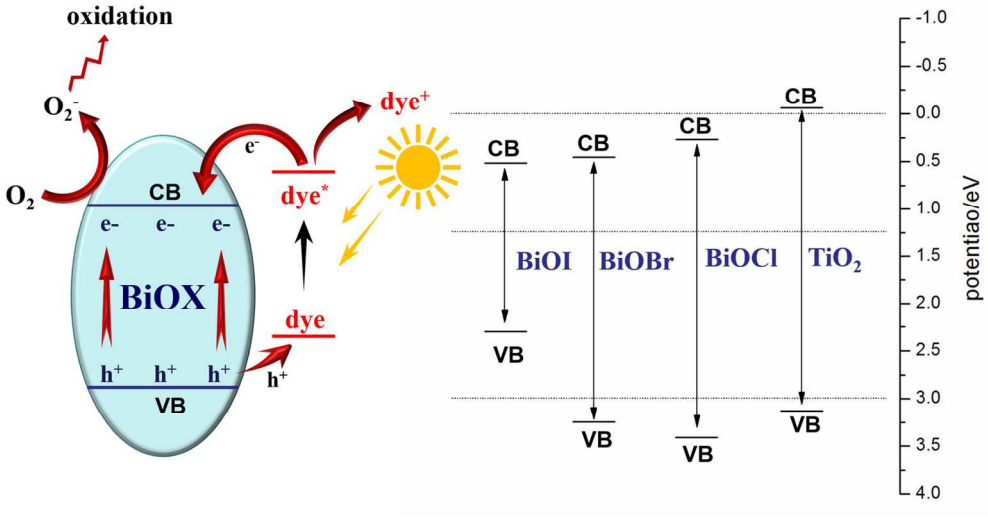

The level position of BiOX and photocatalytic degradation mechanism of RhB.
294x152mm (150 x 150 DPI)